1521-0103/347/3/727–736$25.00
THE JOURNAL OF PHARMACOLOGY AND EXPERIMENTAL THERAPEUTICS

http://dx.doi.org/10.1124/jpet.113.207472
J Pharmacol Exp Ther 347:727–736, December 2013

Hepatic Basolateral Efflux Contributes Significantly to Rosuvastatin Disposition I: Characterization of Basolateral Versus Biliary Clearance Using a Novel Protocol in Sandwich-Cultured Hepatocytes

Nathan D. Pfeifer, Kyunghee Yang, and Kim L. R. Brouwer

Division of Pharmacotherapy and Experimental Therapeutics, UNC Eshelman School of Pharmacy, University of North Carolina at Chapel Hill, Chapel Hill, North Carolina

Received June 26, 2013; accepted September 3, 2013

ABSTRACT

Transporters responsible for hepatic uptake and biliary clearance (CL_{Bile}) of rosuvastatin (RSV) have been well characterized. However, the contribution of basolateral efflux clearance (CL_{BL}) to hepatic and systemic exposure of RSV is unknown. Additionally, the appropriate design of in vitro hepatocyte efflux experiments to estimate CL_{Bile} versus CL_{BL} remains to be established. A novel uptake and efflux protocol was developed in sandwich-cultured hepatocytes (SCH) to achieve desired tight junction modulation while maintaining cell viability. Subsequently, studies were conducted to determine the role of CL_{BL} in the hepatic disposition of RSV using SCH from wild-type (WT) and multidrug resistance-associated protein 2 (Mrp2)-deficient (TR^-) rats in the absence and presence of the P-glycoprotein and breast cancer resistance protein (Bcrp) inhibitor elacridar (GF120918). RSV CL_{Bile} was nearly ablated by GF120918 in TR^- SCH, confirming that Mrp2 and Bcrp are responsible for the majority of RSV CL_{Bile}. Pharmacokinetic modeling revealed that CL_{BL} and CL_{Bile} represent alternative elimination routes with quantitatively similar contributions to the overall hepatocellular excretion of RSV in rat SCH under baseline conditions (WT SCH in the absence of GF120918) and also in human SCH. Membrane vesicle experiments revealed that RSV is a substrate of MRP4 ($K_m = 21 \pm 7$ μM, $V_{max} = 1140 \pm 210$ pmol/min per milligram of protein). Alterations in MRP4-mediated RSV CL_{BL} due to drug-drug interactions, genetic polymorphisms, or disease states may lead to changes in hepatic and systemic exposure of RSV, with implications for the safety and efficacy of this commonly used medication.

Introduction

Hepatic transport plays an important role in the pharmacokinetics and pharmacodynamics of rosuvastatin (RSV) because the liver is the target organ for pharmacologic activity, as well as the primary organ of elimination. Hepatic clearance accounts for 72% of total RSV clearance after an intravenous dose in humans (Martin et al., 2003). A number of transport proteins mediating RSV disposition in the liver have been characterized. Active uptake into hepatocytes is facilitated by multiple organic anion transporting polypeptide (OATP) isoforms; sodium-taurocholate cotransporting polypeptide also has been reported to play a role (Ho et al., 2006; Abe et al., 2008; Kitamura et al., 2008). MRP2 and BCRP are the canalicular proteins primarily responsible for RSV biliary excretion (Huang et al., 2006; Kitamura et al., 2008; Keskitalo et al., 2009; Jemnitz et al., 2010; Hobbs et al., 2012). The role of basolateral transport proteins in RSV efflux from hepatocytes back into sinusoidal blood has not been examined. Hepatic basolateral efflux of RSV could be clinically relevant because impaired hepatic transport resulting from drug-drug interactions and genetic polymorphisms has been shown to alter the pharmacokinetics of RSV (Schneck et al., 2004; Simonson et al., 2004; Zhang et al., 2006; Kiser et al., 2008; Kitamura et al., 2008; Keskitalo et al., 2009; Hobbs et al., 2012). Some of these changes have been associated with altered efficacy (i.e., lowering of low-density lipoprotein) of RSV (Simonson et al., 2003; Tomlinson et al., 2010), and increased systemic exposure has been associated with life-threatening rhabdomyolysis, which is related to statin use in general (Hamilton-Craig, 2001; Thompson et al., 2003). Candidate basolateral efflux transporters for RSV include MRP3 and

This study was supported by the National Institutes of Health National Institute of General Medical Sciences [Grant R01GM41935]. N.D.P. was supported, in part, by the University of North Carolina Royster Society of Fellows.

The content is solely the responsibility of the authors and does not necessarily represent the official views of the National Institutes of Health.

A part of this work was presented at the following workshop: Pfeifer ND and Brouwer KLR (2013) A novel method to elucidate the relative contributions of basolateral efflux clearance versus biliary clearance of rosuvastatin in the sandwich-cultured hepatocyte model. American Association of Pharmaceutical Scientists (AAPS) Workshop on Drug Transporters in ADME; 18–20 March 2013; North Bethesda, MD.

dx.doi.org/10.1124/jpet.113.207472.

ABBREVIATIONS: BCRP, breast cancer resistance protein; CL, clearance; CL_{Bile}, biliary clearance; CL_{BL}, basolateral efflux clearance; CL_{Uptake}, uptake clearance; DHEAS, dehydroepiandrosterone sulfate; $E_2 17\beta G$, estradiol-17-β-D-glucuronide; HBSS, Hanks' balanced salt solution; LDH, lactate dehydrogenase; MRP, multidrug resistance-associated protein; NT, nontransfected; OATP, organic anion transporting polypeptide; RSV, rosuvastatin; SCH, sandwich-cultured hepatocytes; TR^-, Mrp2-deficient; TSB, Tris-sucrose buffer; WT, wild type.

MRP4, which mediate hepatic basolateral excretion of drugs and metabolites, particularly as a compensatory route of excretion under cholestatic conditions (Scheffer et al., 2002; Denk et al., 2004; Gradhand et al., 2008; Chai et al., 2012).

Sandwich-cultured hepatocytes (SCH) typically are used to evaluate vectorial transport into bile and differentiate the roles of active uptake and biliary excretion by modulating tight junctions in the presence (cells + bile) or absence (cells) of divalent cations (Ca^{2+}/Mg^{2+}) in the experimental buffer system (B-CLEAR technology; Qualyst Transporter Solutions, Durham, NC). A number of pharmacokinetic parameters can be calculated from uptake data (typically evaluated over a time period of 10 minutes), including the total substrate accumulation in cells + bile and cells, biliary excretion index, and in vitro clearance for uptake (CL_{Uptake}) and/or biliary excretion (CL_{Bile}), which can be used to predict in vivo clearance values based on scaling factors such as protein content and hepatocellularity (Swift et al., 2010a). Less frequently, the SCH model has been used to assess efflux by preloading cells with substrates (± inhibitors), followed by an efflux phase, and quantifying substrate in cells + bile, cells, and/or appearance in buffer (Jemnitz et al., 2010; Swift et al., 2010b). However, the SCH system has not been characterized under these conditions. In a "simplified" conception of the SCH system, maintenance of tight junctions in the presence of Ca^{2+} would completely seal the bile networks, and efflux experiments would reflect only basolateral efflux clearance (CL_{BL}) (Fig. 1A(i), upper Hepatocyte Scheme. Solid efflux arrows). Efflux in the absence of Ca^{2+} with disrupted tight junctions would reflect basolateral plus biliary efflux and would be greater than efflux in the presence of Ca^{2+} (Fig. 1A(ii-iii), lower Hepatocyte Scheme). In reality, the SCH model is dynamic, with regular and extensive

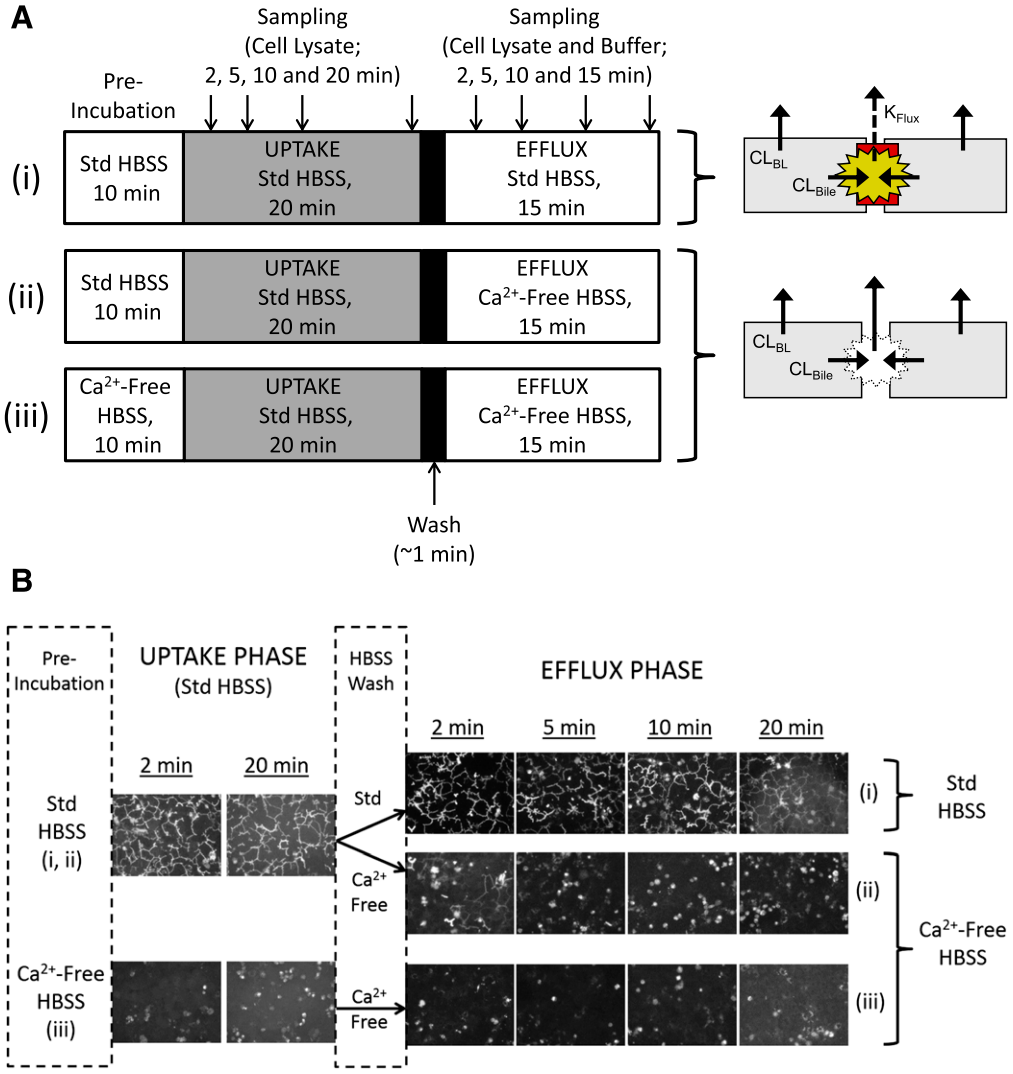

Fig. 1. (A) Scheme depicting preliminary studies designed to evaluate and optimize tight junction modulation throughout the uptake/efflux protocol in the presence of standard (Std; $+Ca^{2+}$) Hanks' balanced salt solution (HBSS) (i) and two potential schemes for conducting efflux in Ca^{2+}-free conditions: (ii) preincubation and uptake exclusively in Std HBSS, followed by a brief wash and efflux in Ca^{2+}-free HBSS; or (iii) maintaining open tight junctions throughout the study period by preincubating in Ca^{2+}-free HBSS, then performing an uptake phase in Std HBSS to provide relief from the removal of Ca^{2+}, followed by a brief wash and efflux in Ca^{2+}-free HBSS. Gray shading represents inclusion of substrate in HBSS during the uptake phase. Cell schemes on the right represent the intended condition of the SCH system during the efflux phase, with arrows depicting the potential pathways leading to substrate efflux from cells + bile (i) and cells (ii and iii), where CL_{BL} represents basolateral efflux, CL_{Bile} represents biliary excretion, and K_{Flux} represents flux from the bile networks (cells + bile only). (B) Fluorescence intensity of carboxydichlorofluorescein (CDF) in bile networks observed after administration of 1 μM CDF diacetate (CDFDA) according to the schemes depicted in (A).

"pulsing" of the bile canaliculi, similar to reports in hepatocyte couplets and cultured hepatocytes (Boyer et al., 1988; Shinoda et al., 1998). Thus, the appearance of substrate in buffer in the presence of Ca^{2+} reflects CL_{BL} plus periodic flux of accumulated substrate within the bile spaces (K_{Flux}; Fig. 1A(i), Hepatocyte Scheme). To deconvolute these data and elucidate the contributions of CL_{Uptake}, CL_{Bile}, CL_{BL}, and K_{Flux}, a pharmacokinetic modeling approach can be applied to SCH data (Liu et al., 1999; Hoffmaster et al., 2005; Lee et al., 2010; Yang and Brouwer, 2012; Pfeifer and Brouwer, 2013).

The purpose of the present studies was to determine the appropriate conditions for conducting efflux studies in the SCH system. A novel uptake/efflux protocol was developed to determine RSV disposition in rat and human SCH. This method, combined with pharmacokinetic modeling, revealed that basolateral and biliary clearance represent alternative elimination routes with a quantitatively similar contribution to the overall hepatocellular excretion of RSV in rat and human SCH. The role and influence of certain transporters in the basolateral and canalicular (biliary) efflux of RSV were explored in the SCH system, as well as in isolated expression systems.

Materials and Methods

All chemicals were purchased from Sigma-Aldrich (St. Louis, MO) unless otherwise stated. Nonradiolabeled RSV was purchased from Toronto Research Chemicals Inc. (Toronto, ON, Canada), MK-571 was purchased from Cayman Chemicals (Ann Arbor, MI). [^{3}H]Estradiol-17-β-D-glucuronide ($E_2$17G) and [^{3}H]dehydroepiandrosterone sulfate (DHEAS) were purchased from PerkinElmer Life and Analytical Sciences (Waltham, MA); [^{3}H]RSV was purchased from American Radiolabeled Chemicals, Inc. (St. Louis, MO). GF120918 (elacridar) was a generous gift from GlaxoSmithKline (Research Triangle Park, NC).

Animals. Male Wistar wild-type (WT) rats (250–350 g) from Charles River Laboratories (Wilmington, MA) or male Mrp2-deficient (TR$^-$) rats bred at the University of North Carolina (250–350 g; breeding stock obtained from Dr. Mary Vore, University of Kentucky, Lexington, KY) were used as donors for hepatocyte studies. Rats were allowed free access to water and food and acclimated for a minimum of 1 week before experimentation. All animal procedures complied with the guidelines of the Institutional Animal Care and Use Committee (University of North Carolina, Chapel Hill, NC). All procedures were performed with the animals under full anesthesia with ketamine/xylazine (140/8 mg/kg i.p.).

Sandwich-Cultured Hepatocytes. Freshly isolated rat and human hepatocytes were seeded in 24-well BioCoat plates (BD Biosciences, San Jose, CA) at a density of 0.35×10^6 cells/well (WT rat and human) or 0.2×10^6 cells/well (TR$^-$ rat). Hepatocytes were overlaid with Matrigel basement membrane matrix (BD Biosciences) in a sandwich configuration and maintained as described previously (Swift et al., 2010a). Human hepatocytes were purchased from Life Technologies (Research Triangle Park, NC) or kindly provided by Life Technologies or Triangle Research Laboratories (Research Triangle Park, NC). Hepatocyte donors consisted of one Caucasian man, one Caucasian woman, and one African American woman, ranging in age from 20 to 55 years; their body mass index was 19–30.8 kg/m^2. On day 4 (rat) or day 7 (human), SCH were preincubated for 10 minutes in 0.5 ml/well standard (Ca^{2+}-containing) or Ca^{2+}-free Hanks' balanced salt solution (HBSS). Incubating SCH in Ca^{2+}/Mg^{2+}-free buffer containing EGTA (hereafter referred to as Ca^{2+}-free HBSS) disrupts the tight junctions that form the bile canalicular networks (B-CLEAR technology; Qualyst Transporter Solutions).

Preliminary studies were performed to optimize the uptake/efflux protocol and evaluate tight junction modulation using two potential schemes for conducting efflux studies in SCH under Ca^{2+}-free conditions [Fig. 1A(ii)]: preincubation and uptake exclusively in standard (+Ca^{2+}) HBSS, followed by a brief wash and efflux in Ca^{2+}-free HBSS or [Fig. 1A(iii)] maintaining open tight junctions throughout the study period by preincubating in Ca^{2+}-free HBSS, then performing an uptake phase in standard HBSS (<30 minutes) to provide relief from the removal of Ca^{2+}, followed by a brief wash and efflux in Ca^{2+}-free HBSS. The uptake/efflux protocol described in Fig. 1A was characterized using 1 μM carboxydichlorofluorescein (CDF) diacetate (CDFDA), and fluorescence intensity of CDF in bile networks was observed by serial imaging using a Zeiss Axiovert 100TV inverted fluorescent microscope (Carl Zeiss Inc., Thornwood, NY) as depicted in Fig. 1B.

For uptake and efflux studies with RSV, SCH were treated with 0.1 or 1 μM [^{3}H]RSV (100 nCi/ml) in the absence or presence of GF120918 (0.5 μM) in standard HBSS for 20 minutes at 37°C. After the 20-minute uptake phase, buffers containing RSV were removed, cells were washed twice with 37°C standard or Ca^{2+}-free HBSS buffer without RSV, and the third application of buffer was added to SCH for the 15-minute efflux phase (Fig. 1A). For conditions in the presence of inhibitor, 0.5 μM GF120918 was maintained in the incubation buffer for the duration of the experiment (preincubation, uptake, and efflux phases). Preliminary studies indicated that 0.5 μM GF120918 was sufficient to inhibit RSV biliary excretion in SCH with minimal impact on uptake. RSV accumulation in cells + bile, cells, and medium (standard HBSS or Ca^{2+}-free HBSS buffer) during uptake (2, 5, 10, and 20 minutes) and efflux (2, 5, 10, and 15 minute) phases were determined by terminal sampling of $n = 3$ wells at each time point. In all cases, incubation medium was collected at the end of the incubation period, and cells were washed twice in ice-cold HBSS. Cells were solubilized in 0.3 ml of 0.5% Triton X-100 and radioactivity in cell lysates and buffer samples was quantified by liquid scintillation counting (Packard TriCarb; PerkinElmer Life and Analytical Sciences). Leakage of lactate dehydrogenase (LDH) into buffer during the uptake/efflux protocol was measured to assess cell viability throughout the study period using the LDH Cytotoxicity Detection Kit (Roche Diagnostics, Indianapolis, IN). LDH release was evaluated as a percentage of total cellular LDH content, represented by values measured after complete cell lysis using 0.5% Triton X-100 (Fig. 2).

Pharmacokinetic Modeling. Pharmacokinetic modeling and simulation were used to evaluate RSV disposition in SCH studies and to determine the effects of GF120918 and loss of Mrp2 function on RSV hepatobiliary disposition in rat SCH. A model scheme incorporating linear parameters governing RSV flux (Fig. 3) was fit to mass versus time data from individual SCH experiments (Figs. 4 and 5). The model fitting was performed with PhoenixWinNonlin, v6.1 (St. Louis, MO) using the stiff estimation method and a proportional model to account for residual error. The following differential equations, which were developed based on the model scheme depicted in Fig. 3, were fit simultaneously to data generated in SCH in the presence of intact and disrupted bile canaliculi for each condition (WT and TR$^-$, ± GF120918):

Mass in buffer (Standard HBSS):

$$\frac{dX^{+}_{Buffer}}{dt} = CL_{BL} \times C^{+}_{Cell} + K_{Flux} \times X_{Bile} - CL_{Uptake} \times C^{+}_{Buffer} - K_{Wash} \times X^{+}_{Buffer} \qquad X^{+}_{Buffer}{}^{\circ} = X_{dose}$$

Mass in buffer (Ca^{2+}-free HBSS):

$$\frac{dX^{-}_{Buffer}}{dt} = (CL_{BL} + CL_{Bile}) \times C^{-}_{Cell} - CL_{Uptake} \times C^{-}_{Buffer} - K_{Wash} \times X^{-}_{Buffer} \qquad X^{-}_{Buffer}{}^{\circ} = X_{dose}$$

Mass in cells:

$$\frac{dX^{+or-}_{Cell}}{dt} = CL_{Uptake} \times C^{+or-}_{Buffer} - (CL_{BL} + CL_{Bile}) \times C^{+or-}_{Cell} \qquad X^{+or-\circ}_{Cell} = 0$$

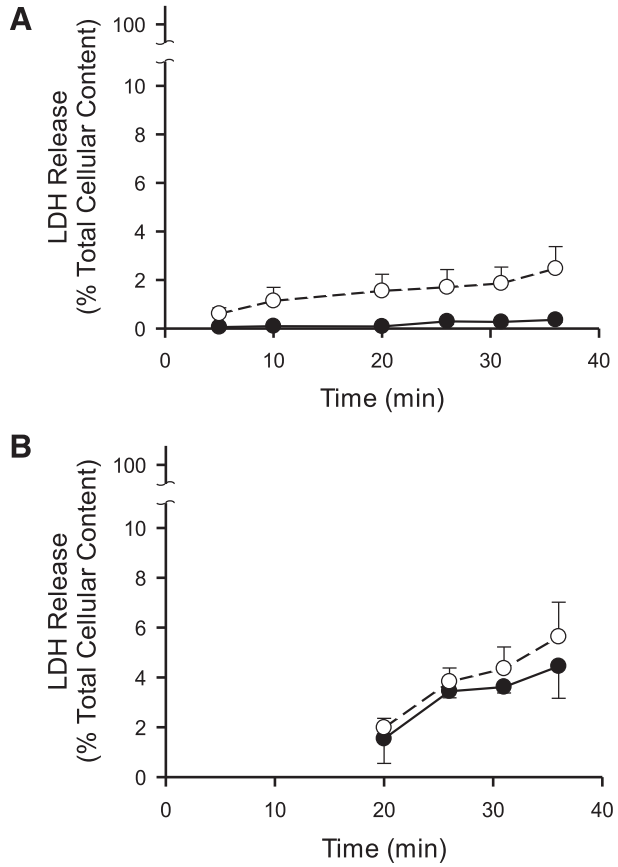

Fig. 2. Lactate dehydrogenase (LDH) release versus time in rat (A) and human (B) sandwich-cultured hepatocyte (SCH) experiments performed according to the scheme depicted in Fig. 1A(i) and (iii) during the uptake and efflux phase, respectively. Closed symbols represent SCH treated in standard ($+Ca^{2+}$) Hanks' balanced salt solution (HBSS) with intact bile networks, whereas open symbols represent cells treated with Ca^{2+}-free HBSS during the preincubation and efflux phase with open bile networks maintained throughout the study period. Data are reported as mean ± S.E. M. (n = 3 SCH preparations in triplicate).

Mass in bile (standard HBSS):

$$\frac{dX_{Bile}}{dt} = CL_{Bile} \times C^{+}_{Cell} - K_{Flux} \times X_{Bile} \qquad X^{\circ}_{Bile} = 0$$

Mass in cells + bile (standard HBSS):

$$\frac{dX_{Cells+Bile}}{dt} = \frac{dX_{Bile}}{dt} + \frac{dX^{+}_{Cell}}{dt}$$

where variables and parameters are defined as in Fig. 3 and K_{wash} was activated for 1.5 minutes at the end of the 20-minute uptake phase and fixed at 1×10^4 min^{-1} based on simulations to eliminate the RSV dose from the buffer compartment and represent the wash step. C_{Cell} represents the intracellular concentration, calculated as X_{Cell}/V_{Cell}, where cellular volume (V_{Cell}) was estimated based on the protein content of each preparation using a value of 7.4 μl/mg protein (Lee and Brouwer, 2010). C_{Buffer} represents the buffer concentration, calculated as X_{Buffer}/V_{Buffer}, where the buffer volume (V_{Buffer}) was constant (0.5 ml). Initial parameter estimates were obtained from noncompartmental analysis of SCH data, where CL_{Uptake} was estimated from the initial (2 minutes) uptake data, $CL_{Uptake} = (dX_{cells+bile}/dt)/C_{Buffer}$ and CL_{BL} and CL_{Bile} were estimated from efflux phase data under Ca^{2+}-free conditions, where $(CL_{BL} + CL_{Bile}) = X^{-}_{Buffer,0-15min}/$ area under the curve $(AUC)_{cells,0-15min}$. K_{Flux}, which represents the flux of substrate out of bile networks in standard HBSS conditions, was estimated initially from simulations using Berkeley-Madonna. Sensitivity analysis of parameter estimates on model output (RSV accumulation in cells + bile and cells at the end of the 20-minute uptake phase; efflux into buffer at the end of the 15-minute efflux phase) was conducted in Berkeley-Madonna v.8.3.11. Parameters representing transport-mediated clearance processes were adjusted in isolation up to 10-fold in either direction of the values describing RSV disposition in WT (control) rat SCH (Table 1); resulting changes in predicted cellular accumulation and efflux into buffer are shown in Fig. 6.

Membrane Vesicles. Human MRP3 plasmid (pcNDA3.1(−)-MRP3) and MRP4 plasmid (pcDNA3.1(−)-MRP4) were kindly provided by Dr. Susan Cole (Queen's University, Kingston, ON, Canada) and Dr. Dietrich Keppler (German Cancer Research Center, Heidelberg, Germany), respectively. Transiently transfected human embryonic kidney cells (HEK293T) were generated and membrane vesicles were prepared as described previously (Leslie et al., 2001). Transport experiments were carried out by a rapid filtration assay as described previously (Ghibellini et al., 2008). In brief, membrane vesicles (10 μg of protein) were incubated at 37°C with test compound in Tris-sucrose buffer (TSB; 50 mM Tris-HCl, 250 mM sucrose, 10 mM $MgCl_2$, 10 mM creatine phosphate, 100 μg/ml creatine kinase, 4 mM ATP or AMP), and 20 μM [^{3}H]$E_2$17G (0.4 μCi/mL) for MRP3, 2 μM [^{3}H]DHEAS (0.7 μCi/ml) for MRP4, or 0.1–100 μM [^{3}H]RSV (0.5 μCi/ml), in a volume of 50 μl. After incubation for 10 minutes, the reaction was stopped by the addition of 0.45 ml of ice-cold TSB and immediately applied to a glass fiber filter (type A/E; Pall Corp., Port Washington, NY) and washed twice with 2 ml of ice-cold TSB. Filters were mixed by vortexing in 5 ml of scintillation fluid, and radioactivity was quantified by liquid scintillation counting (Packard TriCarb; PerkinElmer Life and Analytical Sciences). The ATP-dependent uptake of substrate was calculated by subtracting substrate uptake in the presence of AMP from substrate uptake in the presence of ATP. Membrane vesicles from nontransfected (NT) cells were used to quantify endogenous ATP-dependent uptake of probe substrates. Inhibition data are presented as the percentage of the prototypical substrate ($E_2$17G or DHEAS) uptake in membrane vesicles prepared from cells overexpressing MRP3 or MRP4. Transport of RSV by MRP4 is presented as ATP-dependent uptake, after subtracting endogenous ATP-dependent uptake in NT vesicles. All data are expressed as mean ± S.D. of triplicate determinations in a single experiment.

Data Analysis. The effect of Mrp2 status (WT or TR$^-$) and GF120918 on RSV disposition in SCH experiments was determined by one-way analysis of variance with Tukey's post hoc test. The effect of Mrp2 status was evaluated at each level of inhibitor (absent or present), and the effect of GF120918 was evaluated at each level of Mrp2 status (WT or TR$^-$).

Results

SCH. Preliminary studies conducted to evaluate tight junction modulation and to optimize the uptake/efflux protocol are shown in Fig. 1. After CDFDA administration, fluorescence microscopy confirmed that CDF accumulated in bile networks during the uptake phase following preincubation in standard HBSS [Fig. 1B(i), Uptake Phase), but not in SCH preincubated in Ca^{2+}-free HBSS [Fig. 1B(iii), Uptake Phase] as a result of the disruption of bile networks in the absence of calcium. CDF fluorescence intensity in bile networks was maintained throughout the uptake and efflux phase in the presence of standard HBSS [Fig. 1B(i), Efflux Phase in Standard HBSS]. CDF fluorescence was not visible in bile networks throughout the uptake and efflux phase in Ca^{2+}-free HBSS [Fig. 1B(iii)]. In contrast, disappearance of CDF fluorescence intensity in bile networks after

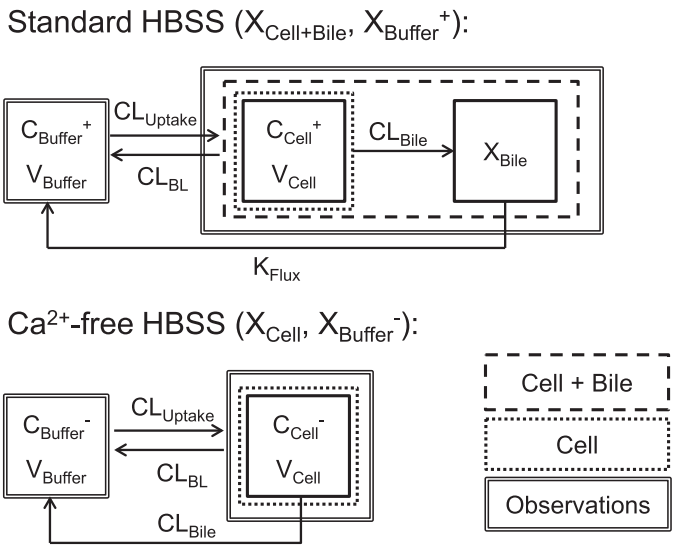

Fig. 3. Model schemes depicting the disposition of rosuvastatin (RSV) in sandwich-cultured hepatocyte (SCH) studies based on the experimental design depicted in Fig. 1A(i) and (iii). X denotes mass of RSV, *V* denotes compartmental volume, *C* denotes compartmental concentration; subscripts on mass, volume and concentration terms denote the corresponding compartment in the model scheme; superscripts represent the presence (+; intact tight junctions, cells + bile) and absence (−, modulated tight junctions, cells) of Ca^{2+} in the incubation buffer; clearance values are designated as CL_{Uptake} for uptake from buffer into hepatocytes, CL_{BL} for efflux from hepatocytes into buffer, CL_{Bile} for canalicular excretion from hepatocytes, and K_{Flux} for flux from bile networks into buffer.

switching from standard HBSS to Ca^{2+}-free HBSS at the wash phase suggested a time frame of ~5 minutes for opening of bile networks [Fig. 1B(ii), Efflux Phase in Ca^{2+}-free HBSS]. As a measure of cell viability during the uptake/efflux protocol, less than 4% and 7% of total cellular LDH content was released over the 35-minute experimental time course in both rat and human SCH, respectively, as shown in Fig. 2.

The mass-time profiles of RSV in cells + bile, cells, and buffer during the optimized uptake/efflux protocol described in Fig. 1A(i) and (iii) are plotted in Fig. 4. After 20-minute treatment (standard HBSS) of WT and TR^{-} SCH with 0.1 or 1 μM [^{3}H]RSV in the absence or presence of GF120918 (0.5 μM), RSV accumulation in cells + bile and cells increased during the uptake phase and decreased during the efflux phase, whereas the appearance in the buffer increased during the efflux phase. RSV accumulation in bile networks (the difference between accumulation in cells + bile and cells) was reduced in Mrp2-deficient TR^{-} SCH, and biliary excretion nearly was ablated in TR^{-} SCH in the presence of GF120918. Parameter estimates recovered from simultaneously fitting differential equations based on the model scheme in Fig. 3 to data at both 0.1 and 1 μM RSV concentrations from independent SCH preparations are listed in Table 1. CL_{Bile} was significantly different between groups (*F*-value 38.2, $P < 0.0001$). The effect of Mrp2 status (WT vs. TR^{-}) was statistically significant in the absence and presence of GF120918; similarly, the effect of GF120918 was statistically significant in WT and TR^{-} SCH. The CL_{BL} term was significantly different between groups (*F*-value = 3.92, $P < 0.048$). However, the individual effect of animal and GF120918 failed to reach significance after correcting for multiple comparisons. CL_{Uptake} was not different between groups (*F*-value = 1.48, $P = 0.28$). There was a trend toward decreased CL_{Uptake} and increased CL_{BL} in TR^{-} compared with WT hepatocytes in both the

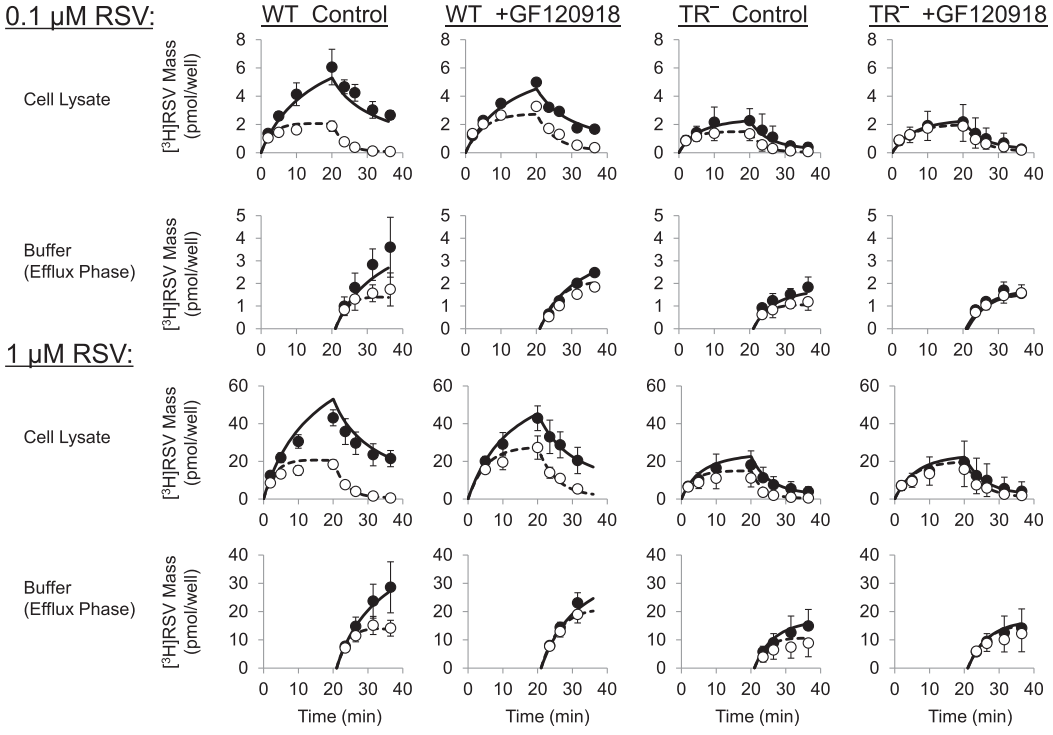

Fig. 4. [^{3}H]Rosuvastatin (RSV) mass versus time data in wild type (WT) and Mrp2-deficient (TR^{-}) rat sandwich-cultured hepatocytes (SCH) in the absence (control) or presence of GF120918 during the uptake and efflux phase. Closed symbols/solid lines represent [^{3}H]RSV in cells + bile (standard HBSS), and open symbols/dashed lines represent [^{3}H]RSV in cells (Ca^{2+}-free HBSS). The simulated mass-time profiles were generated from the relevant equations based on the model scheme depicted in Fig. 3, and the final parameter estimates reported in Table 1. Data (pmol/well) are reported as mean ± S.E.M. (n = 3 to 4 SCH preparations in triplicate per group).

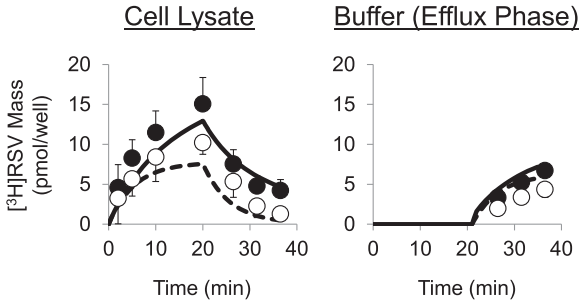

Fig. 5. [^{3}H]Rosuvastatin (RSV) mass versus time data in human sandwich-cultured hepatocytes (SCH) during the uptake and efflux phase. Closed symbols/solid lines represent [^{3}H]RSV mass in cells + bile (standard HBSS), and open symbols/dashed lines represent [^{3}H]RSV mass in cells (Ca^{2+}-free HBSS). The simulated mass-time profiles were generated from the relevant equations based on the model scheme depicted in Fig. 3B and the final parameter estimates reported in Table 1. Data (pmol/well) are reported as mean ± S.E.M. (n = 3 SCH preparations in triplicate).

absence and presence of GF120918. Interestingly, GF120918 tended to decrease both CL_{Uptake} and CL_{BL} in WT and TR^- SCH. The K_{Flux} term was significantly different between groups (F-value = 7.22, $P < 0.01$); K_{Flux} was significantly increased in TR^- SCH in the absence of GF120918. The effect of GF120918 on K_{Flux} was statistically significant in TR^- but not WT SCH. An important finding is that the parameter estimates revealed that CL_{BL} and CL_{Bile} have a similar contribution to the total cellular excretion of RSV under baseline conditions (WT SCH in the absence of GF120918).

Uptake of 1 μM RSV and subsequent efflux were examined in SCH from three human liver preparations (Fig. 4). Parameter estimates recovered from fitting the differential equations based on the model scheme depicted in Fig. 3 to data from independent human SCH preparations are listed in Table 1. CL_{Uptake} was at least an order of magnitude greater than the efflux pathways (CL_{BL} and CL_{Bile}), which were of similar magnitude; CL_{BL} was approximately 3-fold greater than CL_{Bile} in human SCH. K_{Flux} was similar to the value observed in rat SCH.

Sensitivity Analysis. Sensitivity analysis of parameter estimates on model output was conducted; resulting changes in simulated cellular accumulation and efflux into buffer are shown in Fig. 6. Cellular accumulation at the end of the uptake phase was most sensitive to CL_{Uptake} in the absence and presence of Ca^{2+}. The amount of substrate in buffer at the end of the efflux phase was most sensitive to increased CL_{Bile} in Ca^{2+}-free conditions, whereas efflux in the presence of Ca^{2+} was most sensitive to CL_{Uptake} across a range of values and also to increased CL_{BL}. Cellular accumulation and efflux into buffer in the absence of Ca^{2+} were not affected by K_{Flux} since bile networks are disrupted in Ca^{2+}-free HBSS.

MRP3- and MRP4-Mediated Transport in Membrane Vesicles. The inhibitory potential and substrate specificity of RSV for MRP3 and MRP4 were evaluated using membrane vesicles prepared from NT- and MRP-overexpressing HEK293T cells. Pilot studies confirmed that ATP-dependent uptake was linear up to 5 and 2 minutes for the prototypical MRP3 and MRP4 probe substrates, $E_2$17G and DHEAS, respectively (data not shown). ATP-dependent uptake determined at 1 minute was concentration-dependent with a K_m and V_{max} of 23 ± 5 μM and 1700 ± 200 pmol/min per milligram protein, respectively, for $E_2$17G, and 2.9 ± 0.2 μM and 390 ± 40 pmol/min per milligram of protein, respectively, for DHEAS (mean ± S.D.). Coincubation with 50 μM RSV inhibited ATP-dependent transport of the prototypical MRP3 and MRP4 probe substrates, $E_2$17G (20 μM) and DHEAS (2 μM), by 76 ± 2% and 88 ± 5%, respectively (Fig. 7, A and B). By comparison, ATP-dependent transport of $E_2$17G (20 μM) and DHEAS (2 μM) was 77 ± 3% and 88 ± 5% lower in NT membrane vesicles and decreased by 98 ± 2% and 105 ± 3% in the presence of the potent pan-MRP inhibitor, MK-571 (50 μM, Fig. 7, A and B). ATP-dependent transport of 0.1 μM RSV was linear up to ~1 minute and was greater in membrane vesicles from HEK293T cells overexpressing MRP4 and MRP3 compared with NT cells (Fig. 7C). Uptake of RSV at 1 minute in membrane vesicles from MRP4-overexpressing cells was concentration-dependent with a K_m and V_{max} of 21 ± 7 μM and 1140 ± 210 pmol/min per milligram of protein for MRP4

TABLE 1

Summary of recovered parameter estimates and residual error based on the model scheme depicted in Fig. 3 describing rosuvastatin (RSV) disposition in sandwich-cultured hepatocytes (SCH) from wild-type (WT) and Mrp2-deficient (TR^-) rats in the absence (control) or presence of GF120918 and in human SCH

SCH were treated with 0.1 and 1 μM RSV in rat SCH, and 1 μM RSV in human SCH (see Fig. 1A(i) and (iii) for details of incubation conditions) and the model was fit simultaneously to all data from each preparation. Data are presented as mean ± S.D. of individual fits from n = 3 to 4 SCH preparations. A proportional error model was used, with a mean residual error (CV%) of ~20–50% for each parameter and condition (≤ ~100% for individual replicates).

Condition	CL_{Uptake}	CL_{BL}[#]	CL_{Bile}	K_{Flux}
	ml/min/g liver			*min^{-1}*
WT SCH				
Control	9.5 ± 2.7	0.21 ± 0.07	0.23 ± 0.04	0.057 ± 0.029
+GF120918	7.9 ± 1.0	0.16 ± 0.03	0.079 ± 0.017†	0.046 ± 0.007
TR^- SCH				
Control	7.6 ± 1.2	0.34 ± 0.09	0.089 ± 0.025*	0.093 ± 0.008*
+GF120918	6.6 ± 1.6	0.27 ± 0.06	0.018 ± 0.015*†	0.049 ± 0.027†
Human SCH	1.4 ± 0.3	0.10 ± 0.02	0.037 ± 0.015	0.044 ± 0.035

[#] CL_{BL} was significantly different between groups in rat SCH (F-value = 3.92, $P < 0.048$), but individual effects of Mrp2 status and GF120918 failed to reach significance after correcting for multiple comparisons.

* $P < 0.05$, adjusted: effect of Mrp2 status (WT vs. TR^-) is statistically significant within the same level of inhibitor (control or +GF120918).

† $P < 0.05$, adjusted: effect of GF120918 (absence vs. presence) is statistically significant within the same level of Mrp2 status (WT or TR^-).

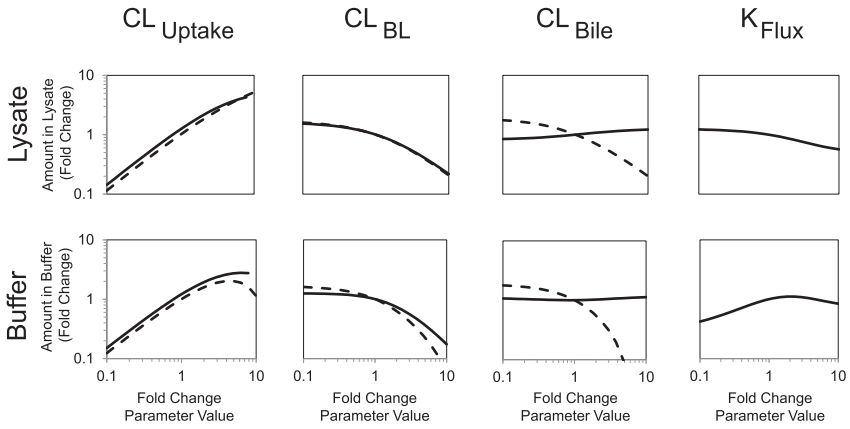

Fig. 6. Sensitivity analysis of parameter estimates determined from the model depicted in Fig. 3. Parameters were altered 10-fold in either direction of the values estimated for mean control data (Table 1), and the -fold change in the predicted model output was examined. Model output included rosuvastatin (RSV) accumulation in cells + bile or cells at the end of the 20-minute uptake phase (lysate; top panel) and RSV efflux into buffer at the end of the 15-minute efflux phase (buffer; bottom panel). Solid lines represent incubations in standard HBSS (cells + bile), and dashed lines represent incubations in Ca^{2+}-free HBSS (cells).

(Fig. 7D). Despite inhibition of MRP3-mediated $E_2$17G transport by 50 μM RSV (Fig. 7A) and apparent MRP3-dependent RSV uptake at low concentrations (Fig. 7C), ATP-dependent uptake of RSV over a range of concentrations in membrane vesicles from MRP3-overexpressing cells was not significantly greater than uptake into vesicles prepared from NT cells (data not shown).

Discussion

The present studies suggest for the first time a significant role for basolateral efflux in the hepatocellular elimination of RSV from rat and human hepatocytes. Examination of this basolateral efflux process was possible using a novel protocol in SCH. Uptake and efflux profiles observed in SCH with maintenance of tight junctions in the closed (standard HBSS, cells + bile) or open (Ca^{2+}-free HBSS, cells) conformation over 35 minutes, and the behavior of the system under these conditions, was characterized for the first time.

At least two potential schemes exist for the design of efflux studies in Ca^{2+}-free conditions in SCH [Fig. 1A(ii) and (iii)]. One is to preincubate and perform the uptake phase in standard ($+Ca^{2+}$) HBSS, followed by a brief wash and efflux in Ca^{2+}-free HBSS [Fig. 1A(ii)] (Jemnitz et al., 2010; Swift et al., 2010b). A limitation of this approach is that substrate accumulation in bile networks during the uptake phase may not be washed away completely before initiating the efflux phase in Ca^{2+}-free HBSS. Based on the disappearance of CDF fluorescence intensity in bile networks [Fig. 1B(ii), Efflux

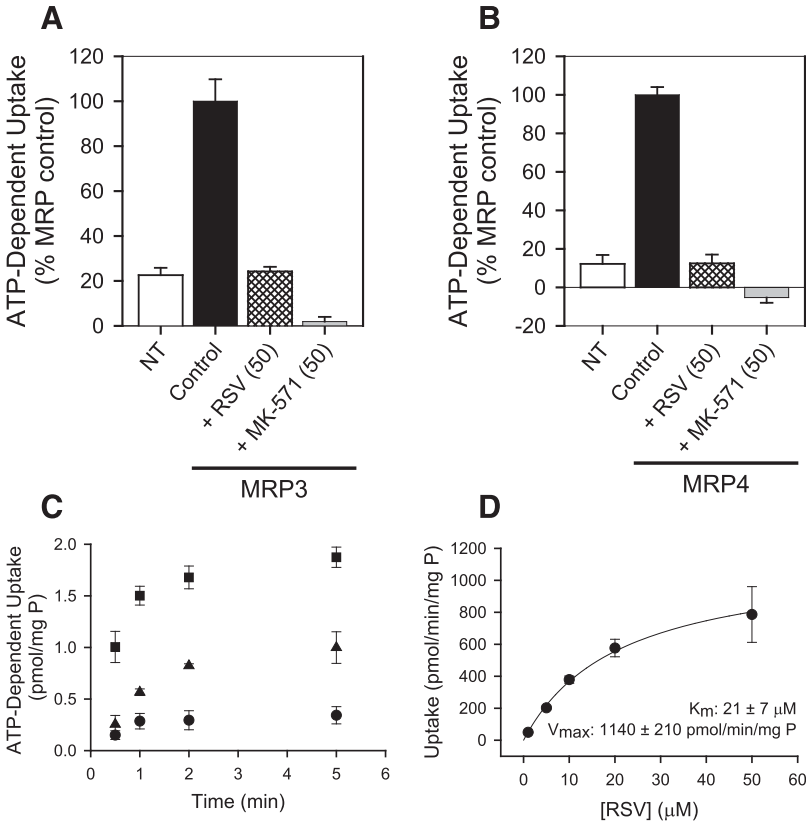

Fig. 7. ATP-dependent uptake of (A) 20 μM [^{3}H]estradiol-17-β-D-glucuronide ($E_2$17G) or (B) 2 μM [^{3}H]dehydroepiandrosterone sulfate (DHEAS) in membrane vesicles from nontransfected (NT) and MRP3- or MRP4-overexpressing (control) human embryonic kidney (HEK293T) cells, respectively, and inhibition by 50 μM rosuvastatin (RSV) and MK-571. (C) Time-dependent transport of [^{3}H]RSV in membrane vesicles from NT (●) MRP3- (▲) and MRP4- (■) overexpressing cells. (D) Concentration-dependent transport of RSV in membrane vesicles from MRP4-overexpressing HEK293T after subtracting endogenous ATP-dependent uptake in vesicles from NT cells; V_{max} and K_m values were obtained from nonlinear regression analysis. In all cases, data represent mean ± S.D. of triplicate measurements in a single experiment.

Phase], the time required for complete opening of canalicular networks is 2–5 minutes. Before this time, efflux into the buffer in Ca^{2+}-free HBSS reflects, in part, content from the opening of bile networks. Another potential design for efflux studies involves maintaining open tight junctions throughout the study period. This is accomplished by preincubating in Ca^{2+}-free HBSS and then performing the uptake phase in standard HBSS to provide relief from prolonged exposure to Ca^{2+}-free conditions, followed by a brief wash and efflux in Ca^{2+}-free HBSS [Fig. 1A(iii)]. A limitation with this method is potential resealing of the tight junctions during Ca^{2+} repletion throughout the uptake phase (Liu et al., 1999). However, imaging with CDF suggests that resealing of the tight junctions allowing substrate accumulation in the bile networks is minimal over the 20-minute uptake phase [Fig. 1B(iii)]. Therefore, based on the data generated, preincubating SCH in standard or Ca^{2+}-free HBSS before performing the uptake phase in standard HBSS, followed by a brief wash and then efflux in standard or Ca^{2+}-free HBSS [Fig. 1A(i) and (iii)], is the most appropriate method for conducting efflux studies in the SCH system. It should be noted that pharmacokinetic modeling of the data is required to differentiate the individual contributions of CL_{BL} and CL_{Bile}. A potential concern when maintaining open tight junctions in SCH studies is the loss of cell viability resulting from prolonged or repeated exposure to Ca^{2+}-free HBSS (Swift et al., 2010a). In the present study, less than 4 and 7% of total cellular LDH content was released over the 35-minute uptake/efflux protocol in rat and human SCH, respectively (Fig. 2).

RSV cellular accumulation and appearance in buffer were simulated to reflect 10-fold changes in parameter estimates describing RSV disposition in rat SCH (Table 1, WT control). The simulated data reported in Fig. 6 include RSV accumulation in cells + bile and cells at the end of the 20-minute uptake phase, as well as the mass of RSV in buffer at the end of the 15-minute efflux phase. As expected, the simulated data were least sensitive to changes in the K_{Flux} parameter, which was estimated solely from standard HBSS conditions because this process is absent in Ca^{2+}-free conditions. Cellular accumulation at the end of the uptake phase was most sensitive to CL_{Uptake}. The amount of substrate in buffer at the end of the efflux phase was most sensitive to increased CL_{Bile} and CL_{BL} in Ca^{2+}-free HBSS, whereas efflux in standard HBSS was most sensitive to CL_{Uptake} values, and also to increased CL_{BL}. Interestingly, efflux into buffer was inversely proportional to CL_{BL}, and also CL_{Bile} in Ca^{2+}-free HBSS. This may seem paradoxical until one considers that greater efflux will decrease cellular accumulation during the uptake phase, which drives substrate appearance in buffer during the efflux phase. These findings illustrate the power of a modeling and simulation approach to analyze and interpret the data and to characterize and understand more fully the SCH system under conditions used to perform efflux studies.

SCH data, combined with pharmacokinetic modeling, revealed that CL_{BL} and CL_{Bile} represent alternative pathways with a quantitatively similar contribution to the total hepatocellular excretion of RSV under normal conditions in rat SCH; CL_{BL} was ~3-fold greater than CL_{Bile} in human SCH. The effects of modulating Mrp2 and Bcrp function using TR^- SCH and GF120918, respectively, were consistent with previous reports suggesting that each canalicular transporter contributes to a similar degree and together constitute approximately 90–95% of RSV biliary excretion in rat liver (Kitamura et al., 2008; Hobbs et al., 2012). GF120918 tended to inhibit both CL_{Uptake} and CL_{BL} in rat SCH experiments, consistent with the promiscuous nature of transporter substrates and inhibitors. CL_{Uptake} tended to decrease and CL_{BL} tended to increase in TR^- compared with WT SCH, consistent with the hepatoprotective compensatory changes that would be expected in the setting of impaired biliary excretion. Indeed, it has been shown that NTCP expression is downregulated and Mrp3 upregulated in livers from TR^- compared with WT rats (Johnson et al., 2006).

Transporter expression and function have been reported to change over time in rat SCH. Namely, OATP expression and function in rat SCH is decreased by 4- to 5-fold over days in culture (Kotani et al., 2011; Tchaparian et al., 2011). Therefore, RSV CL_{Uptake} likely is underestimated in rat SCH (Table 1); in contrast, OATP-mediated CL_{Uptake} in human SCH appears to be maintained over days in culture (Kotani et al., 2011). Bcrp and Mrp2 expression have been reported to increase and decrease, respectively, in rat SCH compared with liver tissue (Li et al., 2009a,b, 2010). Therefore, the effects of these changes may have minimal overall impact on RSV CL_{Bile}. Available data suggest that expression of MRP3 and MRP4 in rat and human SCH may be relatively stable over days in culture (Swift et al., 2010a; Ohtsuki et al., 2012; Schaefer et al., 2012). However, robust quantitative proteomics data for transport proteins that mediate CL_{BL} are not yet available. In addition, the CL_{BL} and CL_{Uptake} parameters in Table 1 represent both active and passive components of the transport process. Given these limitations, whole liver data are needed to aid in vitro-in vivo correlation of the CL_{BL} pathway. In addition, physiologically based pharmacokinetic modeling has been used to correlate data in human SCH to available in vivo data (Jones et al., 2012).

Two candidate transporters that could contribute to the basolateral excretion of RSV were examined in membrane vesicles prepared from nontransfected HEK293T cells and HEK293T cells overexpressing MRP3 and MRP4. MRP3 and MRP4 transport was characterized using the prototypical substrates, $E_2$17G and DHEAS, respectively; K_m estimates were similar to values previously reported (Zelcer et al., 2001, 2003). RSV (50 μM) inhibited the MRP3- and MRP4-mediated transport of prototypical substrates to a similar extent as the prototypical pan-MRP inhibitor MK-571 (Fig. 7, A and B). Further studies performed to evaluate the ability of MRP3 and MRP4 to transport RSV directly demonstrated that time- and ATP-dependent uptake in membrane vesicles prepared from MRP3- and MRP4-overexpressing cells was greater than in vesicles from NT cells (Fig. 7C). Concentration-dependent uptake revealed that RSV was transported by MRP4 with a K_m of ~21 μM. Unbound RSV concentrations in human liver are likely to be below this K_m value, despite efficient hepatic uptake and accumulation. The mean steady-state RSV maximum total plasma concentration in humans is ~50 ng/ml (0.1 μM) after an 80-mg daily oral dose (Warwick et al., 2000; Cooper et al., 2003). Accumulation (Kp) of total RSV in human and rat hepatocytes in vitro was ~20-fold in the present study, consistent with previous reports (Nezasa et al., 2003), and ~20- to 45-fold accumulation in rat liver in vivo (Nezasa et al., 2002), leading to estimated hepatocellular RSV concentrations of $\leq$5 μM in humans. At present, the contribution of other transport proteins and passive

diffusion to RSV CL_{BL} in SCH cannot be ruled out because specific MRP4 inhibitors have not been identified.

A novel uptake and efflux protocol was developed in SCH that revealed the significant contribution of basolateral efflux to the hepatocellular excretion of RSV in rat and human hepatocytes. When combined with a modeling approach, this experimental paradigm can be used to elucidate the relative contribution of CL_{BL} as well as CL_{Bile}. RSV is a substrate for human MRP4, which likely contributes to the basolateral efflux of RSV in human liver. An important note is that MRP4-mediated efflux of RSV may be impaired due to patient-specific factors such as drug-drug interactions, genetic variation, or disease states. Altered function of MRP4 may lead to changes in hepatic and systemic exposure of RSV, which may impact the efficacy and safety of RSV. The involvement of hepatic basolateral efflux in drug disposition remains largely unrecognized except in the case of hepatically derived drug conjugates. Important next steps will be to assess the basolateral efflux of RSV and other drugs in whole liver to ascertain the potential role of this pathway in vivo, and the predictive capability of the current SCH method.

Acknowledgments

The authors thank Certara, as a member of the Pharsight Academic Center of Excellence Program, for providing Phoenix WinNonlin software to the Division of Pharmacotherapy and Experimental Therapeutics, UNC Eshelman School of Pharmacy.

Authorship Contributions

Participated in research design: Pfeifer, Yang, Brouwer.

Conducted experiments: Pfeifer, Yang.

Performed data analysis: Pfeifer, Yang, Brouwer.

Wrote or contributed to the writing of the manuscript: Pfeifer, Yang, Brouwer.

References

Abe K, Bridges AS, Yue W, and Brouwer KLR (2008) In vitro biliary clearance of angiotensin II receptor blockers and 3-hydroxy-3-methylglutaryl-coenzyme A reductase inhibitors in sandwich-cultured rat hepatocytes: comparison with in vivo biliary clearance. *J Pharmacol Exp Ther* **326**:983–990.

Boyer JL, Gautam A, and Graf J (1988) Mechanisms of bile secretion: insights from the isolated rat hepatocyte couplet. *Semin Liver Dis* **8**:308–316.

Chai J, He Y, Cai SY, Jiang Z, Wang H, Li Q, Chen L, Peng Z, He X, and Wu X, et al. (2012) Elevated hepatic multidrug resistance-associated protein 3/ATP-binding cassette subfamily C 3 expression in human obstructive cholestasis is mediated through tumor necrosis factor alpha and c-Jun NH2-terminal kinase/stress-activated protein kinase-signaling pathway. *Hepatology* **55**:1485–1494.

Cooper KJ, Martin PD, Dane AL, Warwick MJ, Raza A, and Schneck DW (2003) Lack of effect of ketoconazole on the pharmacokinetics of rosuvastatin in healthy subjects. *Br J Clin Pharmacol* **55**:94–99.

Denk GU, Soroka CJ, Takeyama Y, Chen WS, Schuetz JD, and Boyer JL (2004) Multidrug resistance-associated protein 4 is up-regulated in liver but down-regulated in kidney in obstructive cholestasis in the rat. *J Hepatol* **40**:585–591.

Ghibellini G, Leslie EM, Pollack GM, and Brouwer KLR (2008) Use of Tc-99m mebrofenin as a clinical probe to assess altered hepatobiliary transport: integration of in vitro, pharmacokinetic modeling, and simulation studies. *Pharm Res* **25**:1851–1860.

Gradhand U, Lang T, Schaeffeler E, Glaeser H, Tegude H, Klein K, Fritz P, Jedlitschky G, Kroemer HK, and Bachmakov I, et al. (2008) Variability in human hepatic MRP4 expression: influence of cholestasis and genotype. *Pharmacogenomics J* **8**:42–52.

Hamilton-Craig I (2001) Statin-associated myopathy. *Med J Aust* **175**:486–489.

Ho RH, Tirona RG, Leake BF, Glaeser H, Lee W, Lemke CJ, Wang Y, and Kim RB (2006) Drug and bile acid transporters in rosuvastatin hepatic uptake: function, expression, and pharmacogenetics. *Gastroenterology* **130**:1793–1806.

Hobbs M, Parker C, Birch H, and Kenworthy K (2012) Understanding the interplay of drug transporters involved in the disposition of rosuvastatin in the isolated perfused rat liver using a physiologically-based pharmacokinetic model. *Xenobiotica* **42**:327–338.

Hoffmaster KA, Zamek-Gliszczynski MJ, Pollack GM, and Brouwer KLR (2005) Multiple transport systems mediate the hepatic uptake and biliary excretion of the metabolically stable opioid peptide [D-penicillamine2,5]enkephalin. *Drug Metab Dispos* **33**:287–293.

Huang L, Wang Y, and Grimm S (2006) ATP-dependent transport of rosuvastatin in membrane vesicles expressing breast cancer resistance protein. *Drug Metab Dispos* **34**:738–742.

Jemnitz K, Veres Z, Tugyi R, and Vereczkey L (2010) Biliary efflux transporters involved in the clearance of rosuvastatin in sandwich culture of primary rat hepatocytes. *Toxicol In Vitro* **24**:605–610.

Johnson BM, Zhang P, Schuetz JD, and Brouwer KLR (2006) Characterization of transport protein expression in multidrug resistance-associated protein (Mrp) 2-deficient rats. *Drug Metab Dispos* **34**:556–562.

Jones HM, Barton HA, Lai Y, Bi YA, Kimoto E, Kempshall S, Tate SC, El-Kattan A, Houston JB, and Galetin A, et al. (2012) Mechanistic pharmacokinetic modeling for the prediction of transporter-mediated disposition in humans from sandwich culture human hepatocyte data. *Drug Metab Dispos* **40**:1007–1017.

Keskitalo JE, Zolk O, Fromm MF, Kurkinen KJ, Neuvonen PJ, and Niemi M (2009) ABCG2 polymorphism markedly affects the pharmacokinetics of atorvastatin and rosuvastatin. *Clin Pharmacol Ther* **86**:197–203.

Kiser JJ, Gerber JG, Predhomme JA, Wolfe P, Flynn DM, and Hoody DW (2008) Drug/Drug interaction between lopinavir/ritonavir and rosuvastatin in healthy volunteers. *J Acquir Immune Defic Syndr* **47**:570–578.

Kitamura S, Maeda K, Wang Y, and Sugiyama Y (2008) Involvement of multiple transporters in the hepatobiliary transport of rosuvastatin. *Drug Metab Dispos* **36**: 2014–2023.

Kotani N, Maeda K, Watanabe T, Hiramatsu M, Gong LK, Bi YA, Takezawa T, Kusuhara H, and Sugiyama Y (2011) Culture period-dependent changes in the uptake of transporter substrates in sandwich-cultured rat and human hepatocytes. *Drug Metab Dispos* **39**:1503–1510.

Lee JK and Brouwer KR (2010) Determination of intracellular volume of rat and human sandwich-cultured hepatocytes (Abstract ID 1595). *The Toxicologist. Toxicol Sci* **114 (Suppl)**:339.

Lee JK, Marion TL, Abe K, Lim C, Pollack GM, and Brouwer KLR (2010) Hepatobiliary disposition of troglitazone and metabolites in rat and human sandwich-cultured hepatocytes: use of Monte Carlo simulations to assess the impact of changes in biliary excretion on troglitazone sulfate accumulation. *J Pharmacol Exp Ther* **332**:26–34.

Leslie EM, Mao Q, Oleschuk CJ, Deeley RG, and Cole SP (2001) Modulation of multidrug resistance protein 1 (MRP1/ABCC1) transport and atpase activities by interaction with dietary flavonoids. *Mol Pharmacol* **59**:1171–1180.

Li N, Palandra J, Nemirovskiy OV, and Lai Y (2009a) LC-MS/MS mediated absolute quantification and comparison of bile salt export pump and breast cancer resistance protein in livers and hepatocytes across species. *Anal Chem* **81**: 2251–2259.

Li N, Singh P, Mandrell KM, and Lai Y (2010) Improved extrapolation of hepatobiliary clearance from in vitro sandwich cultured rat hepatocytes through absolute quantification of hepatobiliary transporters. *Mol Pharm* **7**:630–641.

Li N, Zhang Y, Hua F, and Lai Y (2009b) Absolute difference of hepatobiliary transporter multidrug resistance-associated protein (MRP2/Mrp2) in liver tissues and isolated hepatocytes from rat, dog, monkey, and human. *Drug Metab Dispos* **37**:66–73.

Liu X, LeCluyse EL, Brouwer KR, Lightfoot RM, Lee JI, and Brouwer KLR (1999) Use of Ca^{2+} modulation to evaluate biliary excretion in sandwich-cultured rat hepatocytes. *J Pharmacol Exp Ther* **289**:1592–1599.

Martin PD, Warwick MJ, Dane AL, Brindley C, and Short T (2003) Absolute oral bioavailability of rosuvastatin in healthy white adult male volunteers. *Clin Ther* **25**:2553–2563.

Nezasa K, Higaki K, Takeuchi M, Nakano M, and Koike M (2003) Uptake of rosuvastatin by isolated rat hepatocytes: comparison with pravastatin. *Xenobiotica* **33**: 379–388.

Nezasa K, Takao A, Kimura K, Takaichi M, Inazawa K, and Koike M (2002) Pharmacokinetics and disposition of rosuvastatin, a new 3-hydroxy-3-methylglutaryl coenzyme A reductase inhibitor, in rat. *Xenobiotica* **32**:715–727.

Ohtsuki S, Schaefer O, Kawakami H, Inoue T, Liehner S, Saito A, Ishiguro N, Kishimoto W, Ludwig-Schwellinger E, and Ebner T, et al. (2012) Simultaneous absolute protein quantification of transporters, cytochromes P450, and UDP-glucuronosyltransferases as a novel approach for the characterization of individual human liver: comparison with mRNA levels and activities. *Drug Metab Dispos* **40**: 83–92.

Pfeifer ND and Brouwer KLR (2013) A novel method to elucidate the relative contributions of basolateral efflux clearance versus biliary clearance of rosuvastatin in the sandwich-cultured hepatocyte model in: *American Association of Pharmaceutical Scientists (AAPS) Workshop on Drug Transporters in ADME*; 18–20 March 2013; North Bethesda, MD.

Schaefer O, Ohtsuki S, Kawakami H, Inoue T, Liehner S, Saito A, Sakamoto A, Ishiguro N, Matsumaru T, and Terasaki T, et al. (2012) Absolute quantification and differential expression of drug transporters, cytochrome P450 enzymes, and UDP-glucuronosyltransferases in cultured primary human hepatocytes. *Drug Metab Dispos* **40**:93–103.

Scheffer GL, Kool M, de Haas M, de Vree JM, Pijnenborg AC, Bosman DK, Elferink RP, van der Valk P, Borst P, and Scheper RJ (2002) Tissue distribution and induction of human multidrug resistant protein 3. *Lab Invest* **82**:193–201.

Schneck DW, Birmingham BK, Zalikowski JA, Mitchell PD, Wang Y, Martin PD, Lasseter KC, Brown CD, Windass AS, and Raza A (2004) The effect of gemfibrozil on the pharmacokinetics of rosuvastatin. *Clin Pharmacol Ther* **75**: 455–463.

Shinoda Y, Suematsu M, Wakabayashi Y, Suzuki T, Goda N, Saito S, Yamaguchi T, and Ishimura Y (1998) Carbon monoxide as a regulator of bile canalicular contractility in cultured rat hepatocytes. *Hepatology* **28**:286–295.

Simonson SG, Martin PD, Mitchell P, Schneck DW, Lasseter KC, and Warwick MJ (2003) Pharmacokinetics and pharmacodynamics of rosuvastatin in subjects with hepatic impairment. *Eur J Clin Pharmacol* **58**:669–675.

Simonson SG, Raza A, Martin PD, Mitchell PD, Jarcho JA, Brown CD, Windass AS, and Schneck DW (2004) Rosuvastatin pharmacokinetics in heart transplant recipients administered an antirejection regimen including cyclosporine. *Clin Pharmacol Ther* **76**:167–177.

Swift B, Pfeifer ND, and Brouwer KLR (2010a) Sandwich-cultured hepatocytes: an in vitro model to evaluate hepatobiliary transporter-based drug interactions and hepatotoxicity. *Drug Metab Rev* **42**:446–471.

Swift B, Yue W, and Brouwer KLR (2010b) Evaluation of (99m)technetium-mebrofenin and (99m)technetium-sestamibi as specific probes for hepatic transport protein function in rat and human hepatocytes. *Pharm Res* **27**:1987–1998.

Tchaparian EH, Houghton JS, Uyeda C, Grillo MP, and Jin L (2011) Effect of culture time on the basal expression levels of drug transporters in sandwich-cultured primary rat hepatocytes. *Drug Metab Dispos* **39**:2387–2394.

Thompson PD, Clarkson P, and Karas RH (2003) Statin-associated myopathy. *JAMA* **289**:1681–1690.

Tomlinson B, Hu M, Lee VW, Lui SS, Chu TT, Poon EW, Ko GT, Baum L, Tam LS, and Li EK (2010) ABCG2 polymorphism is associated with the low-density lipoprotein cholesterol response to rosuvastatin. *Clin Pharmacol Ther* **87**: 558–562.

Warwick MJ, Dane AL, Raza A, and Schneck DW (2000) Single- and multiple-dose pharmacokinetics and safety of the new HMG-CoA reductase inhibitor ZD4522 (Abstract). *Atherosclerosis* **151**:39.

Yang K and Brouwer KLR (2012) Pharmacokinetic modeling and simulation study to predict the impact of troglitazone on the hepatobiliary disposition of taurocholate in rat sandwich-cultured hepatocytes, in *American Association of Pharmaceutical Scientists (AAPS) Annual Meeting*; 13–18 Oct 2012; Chicago, IL.

Zelcer N, Reid G, Wielinga P, Kuil A, van der Heijden I, Schuetz JD, and Borst P (2003) Steroid and bile acid conjugates are substrates of human multidrug-resistance protein (MRP) 4 (ATP-binding cassette C4). *Biochem J* **371**:361–367.

Zelcer N, Saeki T, Reid G, Beijnen JH, and Borst P (2001) Characterization of drug transport by the human multidrug resistance protein 3 (ABCC3). *J Biol Chem* **276**: 46400–46407.

Zhang W, Yu BN, He YJ, Fan L, Li Q, Liu ZQ, Wang A, Liu YL, Tan ZR, and Fen-Jiang, et al. (2006) Role of BCRP 421C>A polymorphism on rosuvastatin pharmacokinetics in healthy Chinese males. *Clin Chim Acta* **373**:99–103.

Address correspondence to: Kim L. R. Brouwer, UNC Eshelman School of Pharmacy, University of North Carolina at Chapel Hill, CB #7569, Chapel Hill, NC 27599-7569. E-mail: kbrouwer@email.unc.edu